Internal Dosimetry Using Data Derived from Autoradiographs

J.L. Humm, R.M. Macklis, K. Bump, L.M. Cobb and L.M. Chin

Joint Center for Radiation Therapy, Boston, Massachusetts; and MRC Radiobiology Unit, Harwell, Didcot, Oxon, United Kingdom

Cancer therapies based on administered radionuclides require accurate information on tumor dose. One of the major factors influencing the distribution of absorbed-dose characteristics is the uniformity of the radiolabel distribution in tissue. To study the effect of nonuniformities, we used image analysis techniques to measure automatically the coordinates of autoradiographic grains (sources) and cell nuclei in cut sections from three different tumors, following treatment with radiolabeled antibodies. The spatial distribution data of sources and cell nuclei from these tumor sections were assessed and the pattern of energy deposition in the cell nuclei calculated, assuming that each autoradiograph grain corresponded to a source of the alpha emitter astatine-211 (^{211}At) or the beta emitter yttrium-90 (^{90}Y). The distribution of deposited energy obtained for the real grain distributions was compared to the distribution assuming a locally uniform source distribution, i.e., simulating grain count averaging as produced by a microdensitometric method within a 100 × 100 μm^2 frame size (frame averaging), and a uniform distribution across the entire section (section averaging). The results show first that when the grain distribution is uniform, the average dose within the section is an adequate estimate of the dose to the cell nuclei. Second, when the grain distribution is nonuniform, the distribution of doses to the cell nuclei is significantly less when calculations use the measured grain coordinates, or frame averaging, than when section averaging is used. Third, when the sources are located on or in the cells, both frame and section averaging produce underestimates of the dose to the cell nuclei.

J Nucl Med 1993; 34:1811–1817

The efficacy and uniformity of tumor cell killing resulting from the radiation dose deposition produced by a radiolabeled tumor targeting agent will depend upon the uniformity of the spatial distribution of the radiolabel through the tumor volume. If the source distribution in a tumor were uniform, then all tumor cells would receive the same dose, (being subject only to stochastic fluctuations). If the source distribution is not uniform, the resultant distribution may produce a significantly different biological response. The magnitude of the variation of dose to individual tumor cells will depend on the spacing of the sources relative to the cells in a given tumor microregion, and the choice of radionuclide. For alpha particles of ranges ≤ 90 μm in tissue, small regional heterogeneities in source distribution can have a significant impact on the local variation of tumor cell doses, whereas the impact for long range beta sources such as yttrium-90 (^{90}Y) (mean range in tissue of 3.9 mm) will be much smaller.

An important question in the field of internal radionuclide dosimetry is how accurately one needs to determine the spatial configuration of the sources to obtain a dose uncertainty less than 10%, for example. The answer to this question obviously will depend on the choice of radionuclide and the distribution of sources relative to the targets in the tissue specimen.

Autoradiographic techniques can be used to visualize radiolabel distribution heterogeneity. In autoradiography, histological sections of the tissues of interest are prepared. These are dipped in a nuclear emulsion, exposed to accumulate sufficient decays and then developed to reveal the grain pattern reflecting the radionuclide distribution in the specimen. High resolution (~1 μ) is necessary for accurate dosimetry of alpha or low energy beta sources with which source location data can be obtained by autoradiography (*1*). For an alpha source, for example, a 1-μ error in the positional coordinates of the source relative to a cell nucleus will result in a 20% error in the dose contribution for a source located at the cell membrane (cell radius = 10 μm and cell nuclear radius = 5 μm). For a beta particle emitter, the dose error for the same uncertainty in the spatial position is also about 20%. The reason for the equivalence of the dose errors for a single alpha or beta source placed close to the target arises because the attenuation of particles is negligible over such small distances. Therefore, any change in dose due to a 1-μm shift in the source position in close proximity to the target results from the inverse square law, i.e., is the effect of geometry only. However, in the practical situation of a cell surrounded by a large number of sources, the error in dose estimate produced by spatial errors in source coordinates will be less significant for the longer range source. This is because the total dose to the cell nucleus results from the sum contribution from all sources within a larger sphere of radius R, where R is the range of the emissions.

Quantitation of autoradiographs has been approached by two methods; microdensitometry and automated grain

Received Mar. 5, 1993; revision accepted June 17, 1993.

For correspondence or reprints contact: J.L. Humm, PhD, Dept. of Medical Physics, Memorial Sloan-Kettering Cancer Center, 1275 York Ave., New York, NY 10021.

counting. The more common procedure is microdensitometry (2,3). In microdensitometry the autoradiograph is scanned with a beam of light, typically about 100 μm in diameter, and the variation in the optical density as a function of position recorded. By establishing a relationship between optical density and the number of silver halide grains per unit area, a two-dimensional map of the activity across the tissue section can be acquired.

There are two potential shortcomings of the microdensitometric approach. First, the calibration of grain count to optical density is only unambiguous for a uniform distribution of grains (activity) on the specimen (when the distribution of particle track intersects with the emulsion obeys Poisson statistics). For a targeted molecule, such as a radiolabeled antibody which may preferentially bind to cell surface antigen, the frequency of grain overlap (i.e., local film saturation), will depend on the actual distribution obtained. Second, microdensitometry only provides information on the distribution of sources, and no information on the relation of the sources to the target cells. Therefore, dosimetric information is obtained devoid of its relation to the cellular structure of the tissue, which is needed to estimate cytotoxicity.

The second method is grain counting. Grain counting is considerably more time-consuming than densitometry because, instead of performing one average measurement per field, N measurements per field are required, where N is the number of grains. It requires about 100 sec to determine the coordinates of the grains and cell nuclei per 100 μm^2 of tissue section compared to about 1 sec to measure the optical density. The speed of dosimetry calculations is an N^2 problem being proportional to both the number of cells and sources. For this reason, an analysis of methods of data reduction and their accuracy for different autoradiographs is highly pertinent.

Grain counting by eye is time-prohibitive, if large areas of a section are to be analyzed. Using image analysis techniques for the automatic recognition of grains and cell nuclei can make feasible the acquisition of large data sets containing many thousands of grains and cells. Such data sets can be used as the basis of microdosimetric calculations.

The objective of this study was to evaluate the dosimetric consequences of different radiolabel distributions from tumor tissue autoradiographs and to focus on two questions:

1. What are the differences in dose distribution between a short range alpha-emitting radionuclide compared to a long-range beta-emitting radionuclide?
2. Do less time-consuming dose averaging techniques provide accurate estimates of the doses to individual cell nuclei?

METHODS

Estimation of the Dose Distribution to Cell Nuclei by Three Methods

We analyzed autoradiographs using an ^{125}I radiolabeled anti-Thy 1.1 antibody (Ox7) from three tumor tissue sections exhibiting distinctly different grain localization patterns. Based on the spatial distributions of sources and cell nuclei, we estimated the dose distribution using two different averaging methods, which were compared with the "exact" distribution calculated using the known coordinates of the sources and cell nuclei.

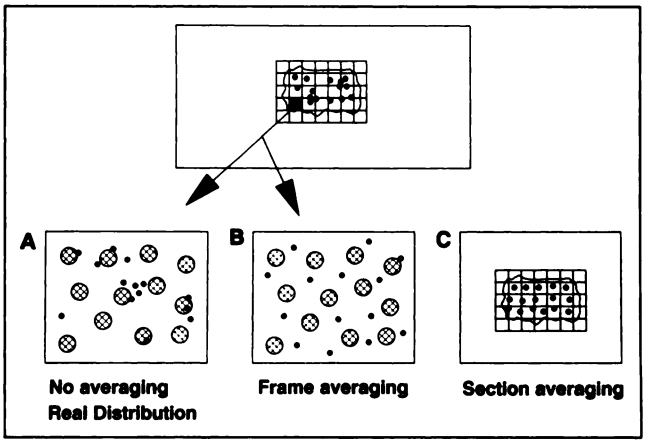

FIGURE 1. A schematic diagram illustrating the three methods used to evaluate the dose distribution to cell nuclei: (A) using the real source and cell nuclear coordinate data (no averaging); (B) by frame averaging, i.e., the number of sources detected within each frame are randomly distributed over the corresponding frame area (100 × 100 μm^2); and (C) by section averaging, i.e., the number of sources detected on the section are randomly distributed over the entire section area.

In the first of the averaging methods, which we subsequently refer to as "frame averaging," the number of grains N per 100 × 100 μm^2 image frame were repositioned uniformly within the bounds of each frame area. This method simulated a densitometric scanning method, in that gross variations of activity across the tissue section are observed, but microscopic effects such as grain-cell association are lost. In the second method, which we subsequently refer to as "section averaging," the grains were assumed to be uniformly distributed across the entire section. The three methods are summarized diagramatically in Figure 1.

In the analysis of the grain coordinates, three assumptions were made:

1. Each grain was assumed to correspond to the site of an ^{125}I decay. This is valid because the short range of the Auger electron emissions released by ^{125}I result has a full width at half maximum of the grain density around the source location of ≤1 μm (4).
2. The grain distribution obtained using a ^{125}I-radiolabeled antibody could be applied for estimating doses from alternative noniodine radiolabeled antibodies. We recognize that this is only approximately true, since published animal studies (5,6) have demonstrated differences in the biodistribution of the radiolabel when the same antibody is radiolabeled with different isotopes.
3. Because histological sections provide information on the source distribution in two dimensions, we assumed that source-to-cell distances from a two-dimensional section were equivalent to the "true" three-dimensional source-to-cell distances. If this assumption is true, the dose distribution to the target cell nuclei is correct. If the tissue structure varies in the third dimension, the dose spectrum derived from a two-dimensional source-to-target configuration will be a distortion of the correct spectrum. The magnitude of

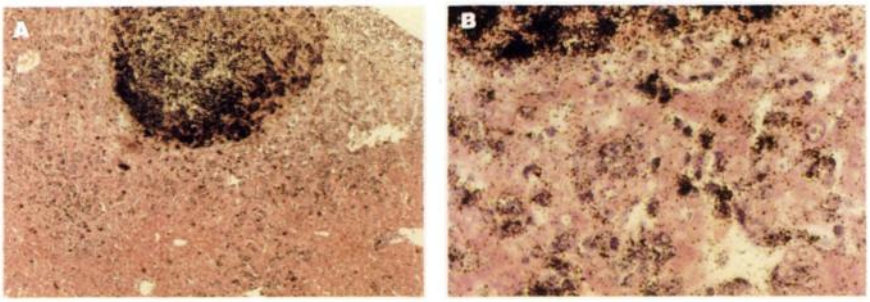

FIGURE 2. (A) Autoradiograph showing the distribution of ^{125}I-radiolabeled tumor specific antibody (Ox-7) in a liver section with a metastatic lymphoma. The magnification is 100×. (B) A region of the same section at 500× magnification. It is at this magnification that the image analysis procedures are used to extract grain and cell nuclear coordinate information.

this distortion will depend on the accuracy with which the section samples the variation of the three-dimensional tissue architecture as well as the radiolabel distribution. This assumption may be more true for a homogeneous tissue such as liver cancers or lymphomas than for highly organized tissue morphologies such as colon or lung cancers.

Autoradiography

Autoradiographs were prepared from three murine tumor model systems: hepatoma, T-cell lymphoma and pneumonocyte type II. Each tumor-bearing animal was injected intravenously with 1.85 MBq of ^{125}I anti-Thy 1.1 antibody and killed after 6 hr. The tumors were removed, processed in paraffin, dipped in Ilford K2 emulsion and exposed for 3 wk. Tissue sections were stained with hematoxylin and eosin. Sections from the three tumors exhibited distinctive differences with regard to the grain distribution pattern.

In the first section, we examined the distribution of the nonspecific anti-Thy 1.1 antibody in a spontaneous murine hepatoma model A166. This was a small, well vascularized, slow-growing tumor with no central necrosis. The distribution of radiolabels (grains) appeared uniform throughout as might be expected for a nonspecific protein in a well vascularized tissue.

The second tumor section was from a T-cell lymphoma T101, which had metastasized to the liver. For this tumor the anti-Thy 1.1 antibody was tumor-cell specific (7). Approximately 50% of the liver cells were malignant T-cells interdispersed uniformly throughout the liver tissue. Figures 2A and 2B show the autoradiograph at two different magnifications. At 100× magnification (Fig. 2A), one can observe a small dense area of autoradiographic grains, corresponding to an area of highly radiolabeled antibody accretion at a tissue necrosis site. At 500× magnification (Fig. 2B), a single field corresponding to one twenty-fifth of Figure 2A is shown. The field's position corresponds to an edge of the necrotic area seen in Figure 2A. One side of the field shows the dense area of overlapping grains (in the necrotic region), and the other side shows a less dense pattern of grains uniformly distributed. The necrotic tissue areas correspond to about 10% of the tissue section and contain approximately 90% of the specimen activity.

The third tumor autoradiograph studied was of a type II pneumonocyte, which arises from the cells that produce lung surfactant. For this tumor, the anti-Thy 1.1 antibody used was nonspecific. Figures 3A and 3B illustrate the autoradiographs of the type II pneumonocyte at 100× and 500× magnification respectively. These autoradiographs demonstrate a different characteristic grain distribution pattern from the hepatoma or lymphoma. Although the antibody was nonspecific, grains can be seen to hug closely to the basement membrane and therefore are in close proximity to tumor cells. Unlike the example autoradiograph of the metastatic lymphoma to the liver, this tumor did not exhibit any significant localized hot pools of activity.

Cell and Grain Detection

A microscope (Reichert Jung Polyvar, Vienna, Austria) with a motorized stage was used to scan and view the specimens with a black and white CCD camera (Cohu, San Diego, CA) mounted on the head of the microscope tube to digitize each field. Using a PC-based image analyzer (Quantimet 570, Leica, Deerfield, IL), image analysis routines were developed to automatically extract the autoradiographic grains and cell nuclei from tissue sections.

Since autoradiograph grains are small (0.3–3 μm^2), tissue sections were viewed under high magnification (500×). The image size was 512 × 480 pixels, and the pixel size calibrated after microscope set-up using a hemocytometer. The field of camera view at the above magnification was 150 × 140 μm^2. A measurement frame of 100 × 100 μm^2 was created in the center of the screen. To prevent miscounting a grain or cell that intersected with the frame border, the same convention was used as is routinely employed in cell-counting with a hemocytometer. This consists of counting any object that intersects with the upper or right frame border, but not those that intersect the lower or left-hand border. After acquisition of data from each frame, the microscope stage is shifted in precisely the amount that corresponds with the width of the frame. Thus, objects that intersected with the left-hand frame border and were not counted on the previous measurement, shift one frame to intersect with the right border where they are counted. Using a motorized stage, each slide was scanned in a raster fashion over 10 × 10 frames corresponding to a sampling area of 1 mm^2 per slide.

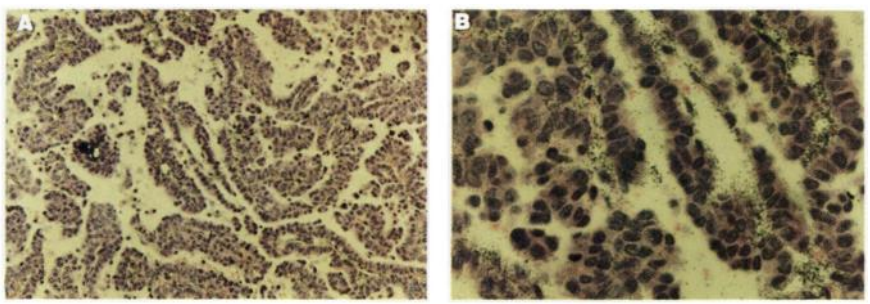

FIGURE 3. (A) Autoradiograph showing the distribution of ^{125}I-radiolabeled nonspecific anti-Thy 1.1 antibody in a type II pneumonocyte at 100× magnification. (B) A region of the same section at 500× magnification.

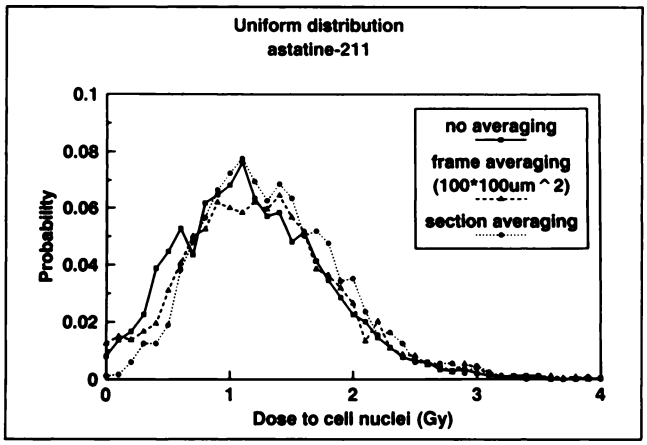

FIGURE 4. The dose distribution for ^{211}At from a uniform distribution of grains derived from an autoradiograph of a hepatoma following the injection of an ^{125}I-radiolabeled nonspecific antibody (anti-Thy 1.1). The dose to the cell nuclei is plotted on the abscissa versus the probability of this dose to an individual cell nucleus on the ordinate.

Cell nuclei are extracted from the image using a series of morphological operations. In brief, the image is coarsely smoothed to remove all small detail, such as grains. The minima of the smoothed image are then sought to identify the most deeply stained regions of the image. By passing the image through a gradient filter, the edges of the cell nuclei are detected, subsequent to which the minima are grown to fill the region contained within the closed gradient boundaries. Automatic cell nuclei detection was accomplished with an accuracy of 75%–90%, dependent on tissue histology. Coordinates of the centroid of each detected cell nucleus were stored in a data file.

Grains were identified by separating the image into the intracellular and extracellular nuclear regions. Grains within cell nuclei were detected by searching for minima underlying the mask of the cell nuclei, as determined above. Extranuclear grains were detected by grey-level segmentation after applying a top hat transform. The accuracy for detection of the autoradiographic grains was ≥90%. To obtain the number of grains in regions of considerable grain overlap, the area of each grain cluster was divided by the mean area of a single grain (0.9 μm^2) determined from tissue section areas containing no grain overlap. Areas of large grain overlap that were lost after application of the top hat transform were encircled by hand. Using grain area to determine grain number results in an underestimation of the true number. This is a limitation of a binary detector such as film.

Calculation of Dose to Cell Nuclei

The doses to all detected cell nuclei on the section were calculated by summing the individual contribution from the coordinates of all detected autoradiographic grains measured on the corresponding area of the section. The dose to cell nuclei was determined, assuming the cell nuclei to be the relevant target for cell sterilization (*8*).

For the alpha emitter dose calculations, the x and y coordinates of each detected grain were used as the site of an ^{211}At disintegration. The coordinates of the centroids of the cell nuclei obtained from tissue section measurements were used as the target data set. Around each centroid, a sphere of 5 μm was constructed representing the cell nucleus. The dose to each cell nucleus was calculated by a Monte Carlo simulation technique as described previously (*9*). In brief, an alpha energy particle was chosen from the decay scheme, weighted by the respective emission energy frequencies. An isotropic emission angle was chosen at random. The entrance and exit coordinate of every alpha particle traversal with a cell nucleus was determined and the energy deposition evaluated for the corresponding segment of the alpha track. By summing all energy deposition events and dividing by the cell nuclear mass, 524×10^{-12} g for a 10-μm diameter unit density sphere, a dose distribution spectrum to the cell nuclei was obtained.

For the beta source ^{90}Y, a composite point kernel for the ^{90}Y emission spectrum was derived using the monenergetic electron dose kernels from Berger (*10,11*). Each autoradiographic grain was scaled to represent an ^{90}Y source of 10^{-3} Bq. The dose rate (Gy/hr) at the center of each nucleus was calculated, by the summation of the dose rate contribution from all sources. Assuming no redistribution of the sources with time, the dose rate distribution was converted to an identical-shape dose distribution in multiplying by the cumulative activity. For a long-range beta source, the energy deposition to the cell nuclei is in charged particle disequilibrium due to the tissue boundaries for small tumor areas. The only contribution to the tumor cell dose considered arises from sources distributed within the tumor area under analysis. Radiation crossfire from adjacent tumor and tissue areas was ignored.

RESULTS

Figure 4 shows a frequency distribution of absorbed dose to cell nuclei derived from a hepatoma (A166) ^{125}I-anti-Thy 1.1 autoradiograph, assuming each grain corresponds to the site of an ^{211}At decay. The mean dose to the cell nuclei (Table 1) as well as the dose distributions for all three methods, schematically illustrated in Figure 1, are in close agreement. Similar results were obtained for ^{90}Y (data not shown). This result is to be expected, when the distribution of grains on the section is uniform.

Figures 5 and 6 show frequency dose distributions to cell nuclei derived from the lymphoma autoradiograph shown in Figure 2 for ^{211}At and ^{90}Y. The impact of areas of high concentration of activity on a slide is to produce a skew distribution of dose to the cell nuclei, for both the no averaging and frame averaging methods, with a high dose tail extending to values many times greater than the mean. Section averaging results in a Poisson distribution of doses

TABLE 1
The Mean Doses in Gray to Cell Nuclei Calculated by the Three Methods*

	No averaging	Frame averaging	Section averaging
Hepatoma (^{211}At)	1.15	1.19	1.29
Hepatoma (^{90}Y)	0.53	0.56	0.61
Lymphoma (^{211}At)	1.61	1.77	2.24
Lymphoma (^{90}Y)	1.67	1.73	1.90
Lung (^{211}At)	2.32	2.13	1.73
Lung (^{90}Y)	1.19	1.14	1.12

*No averaging, frame averaging and section averaging are depicted schematically in Fig. 1.

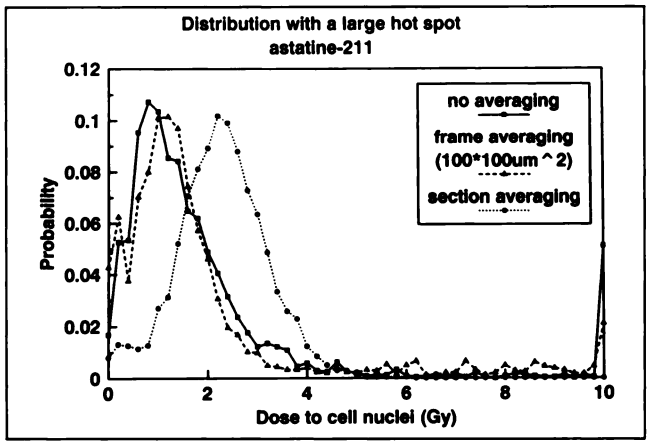

FIGURE 5. The dose distribution for ^{211}At using the grain and cell nuclei distribution data from the autoradiograph of a metastatic lymphoma shown in Figure 2. The dose to the cell nuclei is plotted on the abscissa versus the probability of this dose to an individual cell nucleus on the ordinate. This shows the effect of a "hot spot" in the activity distribution.

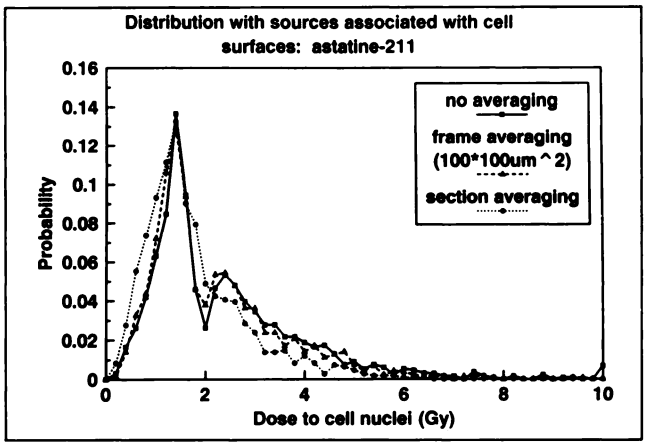

FIGURE 7. The dose distribution for ^{211}At using the grain and cell nuclei distribution data from the autoradiograph of a lung tumor shown in Figure 3. The dose to the cell nuclei is plotted on the abscissa versus the probability of this dose to an individual cell nucleus on the ordinate.

to cell nuclei and the loss of the high dose tail. Dose calculations assuming a uniform source distribution overestimated the mean dose to cell nuclei by 39% for ^{211}At and 14% for ^{90}Y (Table 1). Furthermore, for the section studied in this work, section averaging resulted in a peak dose position which was approximately twice that obtained using no averaging. The calculation for ^{90}Y showed a similar discrepancy as ^{211}At between the location of the dose peak for the no averaging and section averaging methods, in spite of the 3.9 mm mean range for ^{90}Y beta particles.

Figures 7 and 8 show dose distributions to cell nuclei derived from the autoradiograph of the pneumonocyte tumor shown in Figure 3 for ^{211}At and ^{90}Y respectively. The mean dose for the three distributions are given in Table 1. For ^{211}At, the mean dose to the cell nuclei determined without averaging resulted in a 34% greater average dose than obtained by section averaging, and 23% greater by the method of frame averaging. The ^{211}At dose spectrum obtained using the real source coordinate data exhibits a skew distribution in the direction of higher doses. This results from the close association of the sources to some of the tumor cells, as in the case of the lymphoma autoradiograph with the hot spot. When frame or section averaging are performed, detail from the local radionuclide cell association to some cell areas are lost, resulting in a narrowing of the dose distributions and lower mean values (Table 1). Calculations of the average dose for ^{90}Y by the three methods show no significant difference, but the FWHM of the distribution is smallest for the section averaging method.

DISCUSSION

This study presents data on the frequency distribution of dose to cell nuclei obtained by precise analysis of the coordinates of grains and cell nuclei from tumor autoradiographs, alongside the distributions obtained by simpler frame (100 × 100 μm^2) and section averaging methods.

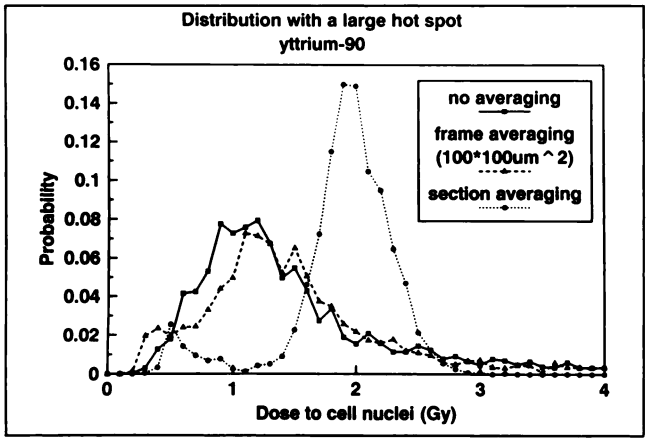

FIGURE 6. The dose distribution for ^{90}Y using the grain and cell nuclei distribution data from the autoradiograph of a metastatic lymphoma shown in Figure 2. The dose to the cell nuclei is plotted on the abscissa versus the probability of this dose to an individual cell nucleus on the ordinate.

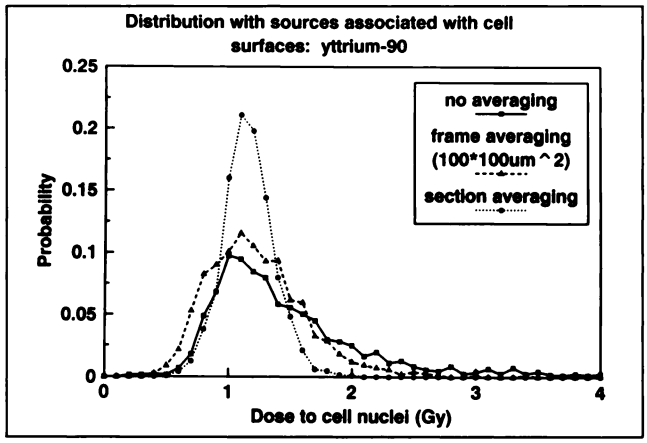

FIGURE 8. The dose distribution for ^{90}Y using the grain and cell nuclei distribution data from the autoradiograph of a lung tumor shown in Figure 3. The dose to the cell nuclei is plotted on the abscissa versus the probability of this dose to an individual cell nucleus on the ordinate.

Note that for a constant number of sources per unit volume, the energy deposited within the entire tumor volume does not change. Yet, variations in the distribution and mean dose to the cell nuclei do occur, due to the dependence of the spatial distribution of sources relative to the cell nuclei. This paper shows the implications of this redistribution for the frequency distribution of doses to the cell nuclei, for a short-range and long-range emitter, in three tumor models.

Short-Range Emitters

For short-range emitters, microscopic analysis of the source distribution relative to the cells is necessary for certain source configurations. If the source distribution is nearly uniform (Fig. 4), then average doses determined by tissue counting are completely adequate, even for alpha emitters provided the absorbed dose is above 1 Gy, the level below which stochastic fluctuations of alpha particles energy deposition require consideration (*12,13*). With increasing levels of source distribution heterogeneity, dose estimates which assume a uniform distribution become increasingly inaccurate.

For the lymphoma section with a single 200-μm hot spot (Fig. 2), frame averaging produced a more accurate distribution of the dose to cell nuclei than section averaging (Fig. 5). Most noticeable in the figure is the shift of the distribution peak to high doses when section averaging is used. This is due to redistribution of grains within the hot spot on the section—where approximately 90% of the activity resides—across the entire specimen. The frequency of high-dose events between 2–4 Gy is slightly greater with no averaging than with frame averaging, an effect due to partial antibody binding outside of the hot spot. However, there is a higher yield of dose events between 4.5–10 Gy for frame averaging. This results from the random repositioning of sources within frames at the edges of the activity hot spot, which produces an increase in the dose to cell nuclei outside the hot spot, and a concomitant decrease in dose to cell nuclei within the hot spot.

The accurate assessment of the fraction of cell nuclei receiving zero or very low doses is of particular significance in radiation therapy, where the objective is to sterilize all clonogenic tumor cells, and tumor cure is governed by the cell population receiving the lowest doses. The yield of zero dose events is highest when frame averaging is used. This is the consequence of the redistribution of grains bound to cells, in low grain density areas of the section, to random nonbound positions, thus increasing the frequency of low dose events. With section averaging, the yield of zero dose events is diminished, because frames of lower grain density are smoothed by adjacent frames of higher grain density.

For the pneumonocyte autoradiograph (Fig. 3), the distribution of dose to the cell nuclei for ^{211}At (Fig. 7), shows the effect of source-cell association or proximity by the presence of a second higher dose peak at 2.5 Gy. This peak persists, but with less prominence, for dose calculations by frame averaging. The structured histology of this tumor and the small frame size results in a large variation in cell number per frame, producing a broadening of the dose distribution to the cell nuclei when frame averaging is employed. As expected, the source-cell association results in a higher frequency of high dose events and a lower probability of low dose events than either averaging method. This kind of cell association heterogeneity can produce significant differences in the distributions for the three methods for short-range emitting isotopes. When source localization occurs preferentially in the cell nuclei, then the cells incorporating the radionuclide can receive doses, potentially orders of magnitude greater than the average tissue dose (*14–16*).

Long-Range Emitters

For ^{90}Y, the dose distributions to cell nuclei calculated with no averaging and frame averaging are in good agreement. The increased precision of the no averaging method was unwarranted for the three autoradiographs studied. Therefore, frame averaging methods to estimate the dose to cell nuclei can be an accurate substitution for microscopic grain analysis. In contrast, the dose distribution produced by section averaging produced a significant overestimate. The similarity of Figures 5 and 6 is due to the dominance of the geometric $1/r^2$ reduction in dose as a function of distance in spite of the large difference in ranges between ^{211}At and ^{90}Y. This result is analogous to the similarity of depth doses for sources of different photon energy in brachytherapy.

In the lymphoma example studied in this work, a single hot spot of 200 μm in diameter had a significant influence on the cellular dose distribution, and yet such hot spots would not be observed in clinical studies by either SPECT or PET imaging. The limited resolution of a gamma camera would smear this distribution uniformly over the voxel. We did not analyze an autoradiograph with multiple small hot spots, but we anticipate that under such conditions there could be a greater discrepancy between the no averaging and frame averaging methods.

For the autoradiograph (Fig. 3) where the activity is approximately uniform (but with cell association) the enhancement of dose to the cell nuclei observed for ^{211}At is averaged out due to the long-range of the ^{90}Y beta rays. The peaks of the dose distributions coincide (Fig. 8), and only the breadth of the distribution by the three calculation methods differs.

CONCLUSIONS

For accurate cellular dosimetry of ^{90}Y, we found it unnecessary to determine the exact spatial coordinates of grains and cell nuclei for the specimens studied. The faster frame averaging method (frame area 100 × 100 μm) provided an estimate of the average dose to cell nuclei within 5% of the real coordinate data for long-range beta sources, unless the sources are concentrated at the cells, and when the intercellular spacing is ≥30 μm (*1*). Section averaging,

which totally ignores source heterogeneity, can give rise to greater errors in the dose estimation to cell nuclei for all sources. Although, for ^{90}Y the average dose to the cell nuclei had an error rate of only 14%, the difference in dose distribution to the tumor cells—which determines survival outcome—could be significantly greater.

When considering short-range emitters, the necessity to evaluate doses to cell nuclei, based on the real coordinate distribution of sources, becomes imperative unless the distribution of sources relative to the viable tumor cell areas is close to uniform. Guidelines for selecting tissue autoradiographs that require detailed microscopic analysis for both alpha and beta radionuclides might include: Autoradiographs for which a large fraction of grains are associated with the cell membranes, or internal to the cell; or autoradiographs containing numerous small, scattered grain clusters (hot spots). For hot spots of area greater than the frame size, frame averaging can be used.

ACKNOWLEDGMENTS

This work was supported by NCI grants No. R01 CA50886 and R29 CA49017 and by the American Cancer Society grant No. ACS-PDT-442.

REFERENCES

1. Humm JL, Cobb LM. Nonuniformity of tumor dose in radioimmunotherapy. *J Nucl Med* 1990;31:75–83.
2. Griffith MH, Yorke ED, Wessels BW, DeNardo GL, Neacy WP. Direct dose confirmation of quantitative autoradiography with micro-TLD measurements for radioimmunotherapy. *J Nucl Med* 1988;29:1795–1809.
3. Eklund KE, Williams JR. A method for quantitative autoradiography over stained sections of tumors exposed in vivo to radiolabeled antibodies. *Int J Radiat Oncol Biol Phys* 1991;21:1635–1642.
4. Rogers AW. *Techniques of autoradiography, third edition*. New York: Elsevier Press, 1979.
5. Khaw BA, Conney J, Edgington T, Strauss HW. Differences in experimental tumor localization of dual-labeled monoclonal antibody. *J Nucl Med* 1986;27:1293–1299.
6. Halpern SE, Hagen PL, Chen A, et al. Distribution of radiolabeled human and mouse monoclonal IgM antibodies in murine models. *J Nucl Med* 1988;29:1688–1696.
7. Cobb LM. Distribution of injected monoclonal antibody in lymphoma-infiltrated spleen. *Leukemia Res* 1989;13:763–769.
8. Munro TR. The relative sensitivity of the nucleus and cytoplasm of the chinese hamster fibroblasts. *Radiat Res* 1970;42:451–470.
9. Humm JL. A microdosimetric model of astatine-211-labeled antibodies for radioimmunotherapy. *Int J Radiat Oncol Biol Phys* 1987;13:1767–1773.
10. Berger MJ. Distribution of absorbed dose around point sources of electrons and beta particles in water and other media. MIRD Pamplet No. 7. *J Nucl Med* 1971;12(suppl. 5):7–23.
11. Berger MJ. Improved point kernels for electron and beta ray dosimetry. Washington DC: US Department of Commerce, National Bureau of Standards. 1973;NBSIR 73-107.
12. Fisher DR. The microdosimetry of monoclonal antibodies with alpha particles. In: Schlafke-Stelson AT, Watson EE, eds. 4th Int Symp Radiopharm Dosim Symp, CONF-851113: Oak Ridge, TN, 1986;446–457.
13. Kellerer AM, Chmelevsky D. Criteria for the applicability of LET. *Radiat Res* 1975;63:226–234.
14. Howell RW, Narra VR, Rao DV, Sastry KSR. Radiobiological effects of intracellular polonium-210 alpha emissions: a comparison with Auger-emitters. *Radiat Prot Dosim* 1990;31:325–328.
15. Humm JL, Chin LM. Cellular dosimetry. In: *Dosimetry of administered radionuclides*. American College of Nuclear Physicians, No. 90-2, Washington DC: ACNP Publications; 1990;306–330.
16. Humm JL, Bagshawe KD, Boxer G, Sharma SK. Tissue dose estimates following the selective uptake of ^{125}IUdR and other radiolabelled thymidine precursors in resistant tumors. *Br J Radiol* 1991;64:45–49.